Effects of surface deposition and droplet injection on film cooling

Jin Wang, Pei Cui, Milan Vujanović , Jakov Baleta, Neven Duić , Zvonimir Guzović

Jin Wang

School of Energy and Environmental Engineering, Hebei University of Technology, Tianjin 300401, China;

***Corresponding author:** wjwcn00@163.com

Phone: +86-22-60435005; Fax: +86-22- 60435279

Pei Cui

School of Energy and Environmental Engineering, Hebei University of Technology, Tianjin 300401, China;

E-mail: cuipei2010@163.com

Milan Vujanović

Department of Energy, Power Engineering and Environment, University of Zagreb, Faculty of Mechanical Engineering and Naval Architecture, Ivana Luč ić a 5, 10002 Zagreb, Croatia

E-mail: milan.vujanovic@fsb.hr

Jakov Baleta

Department of Energy, Power Engineering and Environment, University of Zagreb, Faculty of Mechanical Engineering and Naval Architecture, Ivana Luč ić a 5, 10002 Zagreb, Croatia

E-mail: jakov.baleta@fsb.hr

Zvonimir Guzović

Department of Energy, Power Engineering and Environment, University of Zagreb, Faculty of Mechanical Engineering and Naval Architecture, Ivana Luč ić a 5, 10002 Zagreb, Croatia

E-mail: zvonimir.guzovic@fsb.hr

Neven Duić

Department of Energy, Power Engineering and Environment, University of Zagreb, Faculty of Mechanical Engineering and Naval Architecture, Ivana Luč ić a 5, 10002 Zagreb, Croatia

E-mail: Neven.Duic@fsb.hr

Abstract

In the present research, the influence of the particle dispersion onto the continuous phase in film cooling application was analyzed by means of numerical simulations. The interaction between the water droplets and the main stream plays an important role in the results. The prediction of two-phase flow is investigated by employing the discrete phase model (DPM). The results present heat transfer characteristics in the near-wall region under the influence of mist cooling. The local wall temperature distribution and film cooling effectiveness are obtained, and results show that the film cooling characteristics on the downstream wall are affected by different height of surface deposits. It is also found that smaller deposits without mist injection provide a lower wall temperature and a better cooling performance. With 2% mist injection, evaporation of water droplets improves film cooling effectiveness, and higher deposits cause lateral and downstream spread of water droplets. The results indicate that mist injection can significantly enhance film cooling performance.

Keywords: film cooling; injection; mist cooling; deposition; water droplet; thermal barrier coating

NOMENCLATURE

d	Slot width, m
h	Height of deposition, m
M	Blowing Ratio, $=\rho_i V_i/\rho_\infty V_\infty$
T	Temperature, K
x, y, z	Local coordinates, m

Greek symbols

η	Adiabatic film cooling effectiveness, $=(T_i-T_{aw})/(T_i-T_j)$

Subscripts

aw	Adiabatic wall
i	Mainstream flow
j	Coolant jet

1 Introduction

In order to maintain high thermal efficiency and high power output, Benini [1] indicated that modern gas turbine engines should operate at high temperatures (1200-1600℃). Since such temperatures are much higher than the allowable metal temperatures, it is necessary to cool the turbine components for the safe and durable operation. In order to cool the turbine blade internally and externally, the coolant air is usually extracted from the engine compressor. Polezhaev [2] presented that the transpiration gas-cooled blade concept had demonstrated its ability to provide protection from high temperatures. Hao et al. [3–5] numerically analysed uncoupled thermoelasticity using the Discontinuous Galerkin (DG) finite element method and presented an unconventional formulation for conjugate heat transfer (CHT) problems in gas turbines.

Air film cooling is nowadays commonly employed for the external turbine blade cooling. Discrete holes or several rows of holes with different shapes and inclination angles were investigated in the film cooling technology. Maiteh and Jubran [6] indicated that a favourable pressure gradient reduces the film cooling protection. Koc et al. [7] found that the film cooling effectiveness of a given curved surface depends on the optimum selection of the blowing ratio and maximum curvature height. Asghar and Hyder [8] carried out an analysis of averaged film cooling effectiveness from a row of semi-circular holes, and they found it is almost similar to that of circular holes. Bayraktar and Yilmaz [9] found that maximum cooling efficiency is obtained at the

inclination angle of 30° and blowing ratio of 2.0. Shine et al. [10] showed that increase in the tangential angle may not provide an improvement in film cooling.

However, the air film cooling approaches its limitation. The coolant flow with water mist injection, also called mist cooling, can enhance the film cooling effectiveness due to the following mechanisms [11]: the latent heat of droplet evaporation, direct contact of droplets with the cooling wall and a higher specific heat of both the water steam and water compared to that of air. Li et al. [12] investigated a mist/steam slot jet impinging on a concave surface and simulation results showed that water injection of the 2% coolant flow rate can enhance the adiabatic cooling effectiveness for about 30–50%. Recently, Dhanasekaran and Wang [13,14] revealed the phenomenon of mist secondary flow interaction at bend portion and also performed simulations on both stationary and rotating turbine blades. Jiang et al. [15,16] investigated the effect of various parameters, including mist concentration, droplet diameter (5μ m, 10μ m and 15μ m) and different particle-wall interaction conditions on the improvement of cooling performance. In order to evaluate cooling enhancement, conjugate simulation for the C3X gas turbine vane with leading film holes was also carried out by them. Now scholars point potential merit out in injecting mist into the film-cooling flow, although there are existing problems, such as erosion and corrosion of the turbine components. Mohapatra and Sanjay [17] focused on the comparison of impact of vapour compression and vapour absorption cooling integrated to a cooled gas turbine, and the two methods of inlet air cooling improve the efficiencies of gas turbine cycle by 4.88% and 9.47%, respectively.

For a typical gas turbine, components operate under high temperature, high pressure and high velocity. The harsh environment causes thermal oxidation and surface deterioration, thus reducing component's life. Deposits are formed by various contaminants present in the combustion gases and tend to adhere to surface region around the film cooling holes due to the lower wall temperature in this region. Part of deposits can detach from the surface, peeling off the thermal barrier coating (TBC). Hence, it is important to understand the effect of surface deposition on the performance of film cooling. Bohn and Krewinkel [18] investigated the effect of oxide formation on the cooling effectiveness. They found that the effects of the oxidation on the cooling effectiveness seem to be minimal for the different blowing ratios and that the oxidation layer shows significant influence on the flow field both in the cooling holes and on the plate. Sundaram and Thole [19] indicated that deposits near the hole exit can sometimes improve the cooling effectiveness at the leading edge, but with increased deposition height the cooling deteriorates. Ai et al. [20,21] studied deposition in an accelerated test facility with finely ground coal ash particulates at 1180°C and 180 m/s. In addition, hole spacing influence on the deposition was studied. Sundaram et al. [22] showed a systematic study of factors affecting the delamination energy release rate. They found that transient thermal gradients induce stress gradients through the coating and substrate. Kistenmacher et al. [23] investigated film cooling effectiveness with a thermal barrier coating and deposition in a realistic trench configuration. The results showed that this

configuration was more prone to deposition within the trench, although the trench designs are more helpful to reduce the deposition formation than the round holes.

Since there is almost no literature reporting effects of TBC surface deposition on the film cooling with water droplet injection, present results from the 2D model are compared with the 2D cases without deposition from [12]. Additionally, this work investigates the deposition effect on the film cooling. Moreover, 3D models are also employed to give detailed insights into observed phenomena. Finally, for both 2D and 3D models with mist injection the adiabatic film-cooling effectiveness with different deposition height is investigated.

2 Numerical model and validation

In order to investigate the film cooling effectiveness, both 2D (two-dimensional) and 3D (three-dimensional) meshes are used in numerical simulations as shown in Figure 1. The computational domain is 80d×20d and the 2D model has a slot width (d) of 4mm. The slot is positioned 60d from the exit of the mainstream and vertical height of the jet hole is 1.74d. An inclined angle (α) of 35° is here considered having the optimal value according to [24,25]. A curved cross section is used as an approximation of TBC surface deposition of various heights (0.4h – 0.8h). The streamwise deposit length (w) was 2d for all simulated cases. In the case of 3D model, the domain has a lateral depth of 8d and diameter of the film hole is 8 mm (2d). Similar configurations can be found in [12]. Different curved cross sections representing deposits are used with a varying height of 0.4d, 0.6d and 0.8d. The commercial computational fluid dynamics software ANSYS 15.0 was employed for

numerical calculations. The simulation uses the segregated solver, which employs an implicit pressure-correction scheme. The pressure and velocity were coupled by the SIMPLE algorithm. Discrete phase model (DPM) was used to investigate interaction with continuous phase, where DPM sources are updated every iteration. A second-order upwind scheme was used for spatial discretization of the convective terms and species. The Lagrangian trajectory calculations were adopted for modelling the dispersed phase of droplets, while the impact of the droplets on the continuous phase was handled through the source terms of governing equations. Based on the literature [12], the standard k-ε turbulence model with enhanced wall treatment was used, since it is considered as one of the most robust turbulence models for film cooling flow.

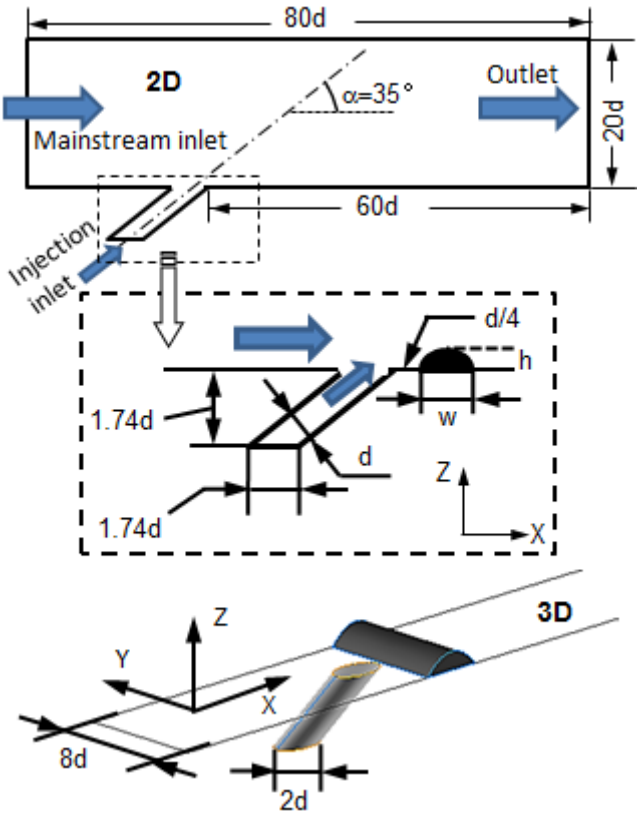

Fig. 1 Computational domain and hole configurations for 2D and 3D

2.1 Continuous phase (air/steam)

In the present study, the standard 2D/3D, time-averaged, steady-state Navier-Stokes equations as well as equations for mass, energy, and species transport are solved. The governing equations of mass, momentum, energy, turbulent kinetic energy and turbulent energy dissipation rate are presented as follows:

Continuity equation:

$$\frac{\partial}{\partial x_i}(\rho u_i) = S_m \tag{1}$$

Momentum equations:

$$\frac{\partial}{\partial x_i}\left(\rho u_i u_j\right) = \rho \vec{g} - \frac{\partial P}{\partial x_j} + \frac{\partial}{\partial x_i}\left(\tau_{ij} - \rho\overline{u_i' u_j'}\right) + F_j \tag{2}$$

Energy equation:

$$\frac{\partial}{\partial x_i}\left(\rho c_p u_i T\right) = \frac{\partial}{\partial x_i}\left(\lambda \frac{\partial T}{\partial x_i} - \rho c_p \overline{u_i' T'}\right) + \left|\mu\Phi + S_h\right| \tag{3}$$

Turbulent kinetic energy k equation:

$$\frac{\partial}{\partial x_i}(\rho k u_i) = \frac{\partial}{\partial x_i}\left(\alpha_k \mu_{eff} \frac{\partial k}{\partial x_j}\right) + G_k + G_b - \rho\varepsilon - Y_M + S_k \tag{4}$$

Rate of energy dissipation ε equation:

$$\frac{\partial}{\partial x_i}(\rho \varepsilon u_i) = \frac{\partial}{\partial x_j}\left(\alpha_\varepsilon \mu_{eff} \frac{\partial \varepsilon}{\partial x_j}\right) + C_{1\varepsilon}\frac{\varepsilon}{k}(G_k + C_{3\varepsilon}G_b) - C_{2\varepsilon}\rho\frac{\varepsilon^2}{k} - R_\varepsilon + S_\varepsilon \ , \tag{5}$$

where S_m is the mass added to the continuous phase from the dispersed second phase and any user-defined sources, F_j are external body forces, $\mu\Phi$ is the viscous dissipation, λ is the thermal conductivity, G_k is the generation of turbulent kinetic energy due to the mean velocity gradients, while G_b is the generation of turbulent kinetic energy due to

buoyancy. Y_M is the contribution of the fluctuating dilatation in compressible turbulence to the overall dissipation rate. Terms $\rho\overline{u_i'u_j'}$, $\rho c_p\overline{u_i'T'}$, μ_t and τ_{ij} represent Reynolds stresses, turbulent heat fluxes, turbulent viscosity and the stress tensor, as follows:

$$-\rho\overline{u_i'u'}_j=\mu_t\left(\frac{\partial u_i}{\partial x_j}+\frac{\partial u_j}{\partial x_i}\right)-\frac{2}{3}\rho k\delta \tag{6}$$

$$\rho c_p\overline{u_i'T'}=-\lambda_t\frac{\partial T}{\partial x_i}=-c_p\frac{\mu_t}{\mathrm{Pr}_t}\frac{\partial T}{\partial x_i} \tag{7}$$

$$\mu_t=\rho C_\mu\frac{k^2}{\varepsilon} \tag{8}$$

$$\tau_{ij}=\mu\left(\frac{\partial u_j}{\partial x_i}+\frac{\partial u_i}{\partial x_j}-\frac{2}{3}\delta_{ij}\frac{\partial u_k}{\partial x_k}\right) \tag{9}$$

The model constants have the following default values according to [26]:

$$\left[C_{1\varepsilon},C_{2\varepsilon},C_\mu,\sigma_k,\sigma_\varepsilon\right]=\left[1.44,1.92,0.09,1.0,1.3\right]$$

2.2 Discrete phase (water droplets)

Since the droplets in the airflow are subject to inertia and hydrodynamic drag, their acceleration is calculated according to Newton's second law:

$$m_p\frac{dv_p}{dt}=F_d+F_g+F_o, \tag{10}$$

where v_p is the droplet velocity vector, F_d is the drag of the fluid on the droplet, F_g is the gravity and F_o represents the other forces, such as virtual mass force, thermophoretic force, Brownian force, Saffman's lift force etc.

First, the droplet is evaporated as a result of high-temperature or low-moisture partial pressure, and then vapour diffuses into the mainstream and transports away. The rate of vaporization is controlled by the concentration difference between the surface and the airstream, and the mass change rate for the droplet can be formulated by:

$$\frac{dm_p}{dt} = \pi d^2 k_c (C_s - C_\infty) \tag{11}$$

where k_c is the mass transfer coefficient and C_s is the vapour concentration at the droplet surface, when it is assumed that the flow over the surface is saturated. C_∞ is the vapour concentration of the bulk flow and it is solved by the transport equations. More details can be found in [12, 27, 28].

2.3 Boundary conditions

For simulations without mist injection, the mainstream is assumed to be dry air and the jet flow is saturated air. Inlet flow velocity and temperature distributions are uniform. The inlet velocities of both the mainstream and the jet are 10 m/s, and the corresponding temperature values are 400 K and 300 K. To analyse the film cooling effectiveness, adiabatic boundary condition was imposed on the bottom wall. The main boundary conditions are presented in the Table 1.

For the mist cooling simulations, water droplets are uniformly injected into the jet parallel to the slot/hole centreline. The mist evaporation in the mainstream is strongly affected by the droplet size. Since Li and Wang [29] showed that injecting 2–10% mist reduces the heat transfer coefficient and the wall temperature, uniform droplets with the size of 10 μm are used to investigate the effect on film cooling performance in the present research. Considering the 2D/3D case, the droplet flow rate is 3.5×10^{-4} kg/s. The injection rate at each location is 1.4×10^{-5} kg/ s for 2% injection (2D cases) and more details can be found in [12].

Table 1 Boundary conditions

Zone	Type	Value
Mainstream	Velocity-inlet	10 m/s, 400 K, DPM: escape
Jet flow	Velocity-inlet	10 m/s, 300 K DPM: escape
Outlet	Pressure-outlet	0 Pa, 400 K,
Droplet injection	/	Size: 1e-5 m, 300 K Flow rate: 3.5e-4 kg/s
Top wall	No-slip	/
Bottom wall	No-slip	/
Side wall	Symmetry	/

2.4 Meshes and convergence

Structured grids are used for 2D and 3D cases, with denser regions near the jet hole and the bottom wall compared to those of the outlet and inlet as shown in Fig. 2. A detailed study of wall grid effect on film cooling effectiveness calculation was shown in [30] where it was concluded that y^+ should be kept between 1 and 5. In present research, the basic model for the 2D case has 13,250 cells and the corresponding y^+ near the bottom wall is 1.9. The grid dependence study for different models with 2% mist is shown in Fig. 3. There is a little impact of the grid resolution on temperature values perpendicular to the wall surface (Y direction), so the model with 13,250 grid cells was used to analyse the film/mist cooling effectiveness for the 2D case. Since the number of cells in the 3D case is more than 1,500,000, no finer grids calculations were attempted.

Moreover, the 3D case with mist (water droplets) injection and surface deposition has a value of y+ = 1.

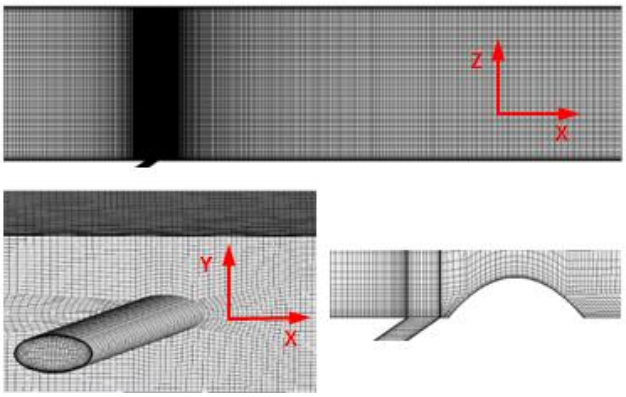

Fig. 2 Computational meshes

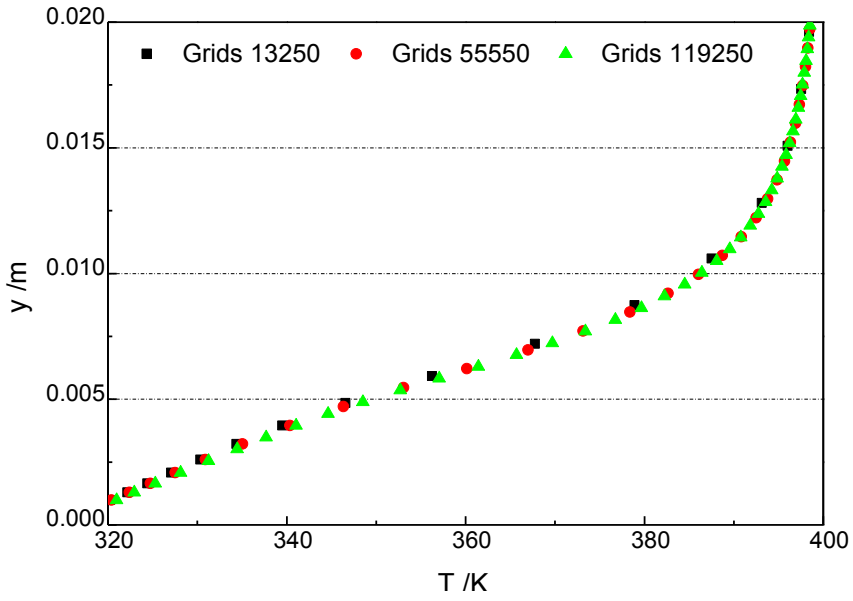

Fig. 3 Grid independence study (2D with 2% mist injection)

The converged results can be obtained by alternating iterations between the continuous and discrete phase. For the continuous phase, 10 iterations are calculated after 2 iterations of the discrete phase. Convergence criteria are met when the results show the mass residual of 10^{-3}, energy residual of 10^{-6}, turbulence kinetic residual of 10^{-5}, and energy dissipation rate residual of 10^{-4}. The average value of the bottom wall

temperature is also monitored, and the deviation of the value must be less than 1% (based on inlet temperature values of the mainstream and the jet flow). More than 2000 iterations are necessary for simulation to converge.

2.5 Model validation

The effect of 2% mist injection on temperature distribution at x=0.1m (x/d=25) is shown in Fig 4. Compared to the reference case of Li et al. [12], the present results for 2D cases, both with and without 2% mist, present a good repeatability. In addition, it seems that 2% mist injection results have obvious influence on the temperature distribution over the wall. The adiabatic wall temperature for 2% mist models is decreased by 15K (inlet temperature difference of 15%). The results indicate that film cooling effectiveness can be improved significantly by the water mist injection.

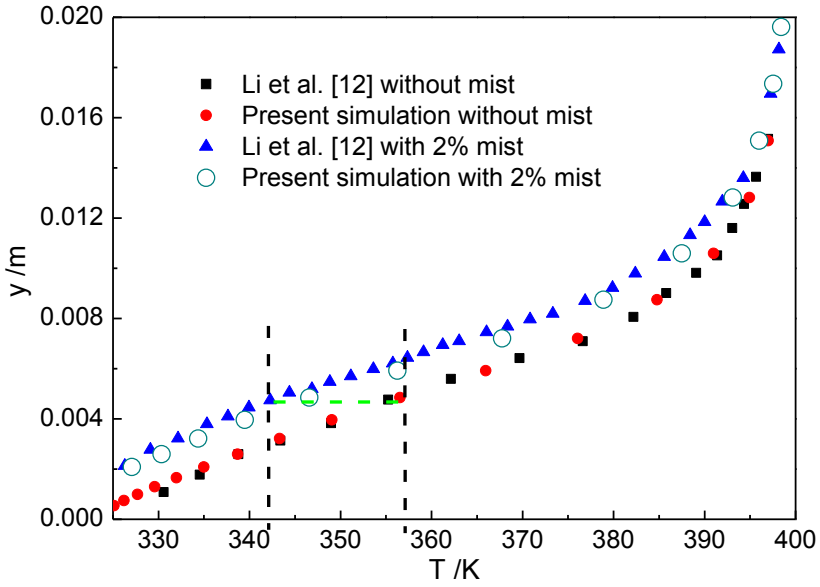

Fig. 4 Model validation (2D with and without 2% mist injection)

3 Results and Discussion

3.1 Temperature distribution

Figure 5 shows temperature distribution for 2D model with and without mist injection and surface deposits. The model without mist and deposition shows that film (air) cooling can provide a wide flow region at low temperature. When 2% mist injection is concerned, the length of a low temperature zone is extended. In other words, mist injection improves the film cooling effectiveness. After surface deposition emerges on the wall the wall temperature distribution is changed by the corresponding distortion.

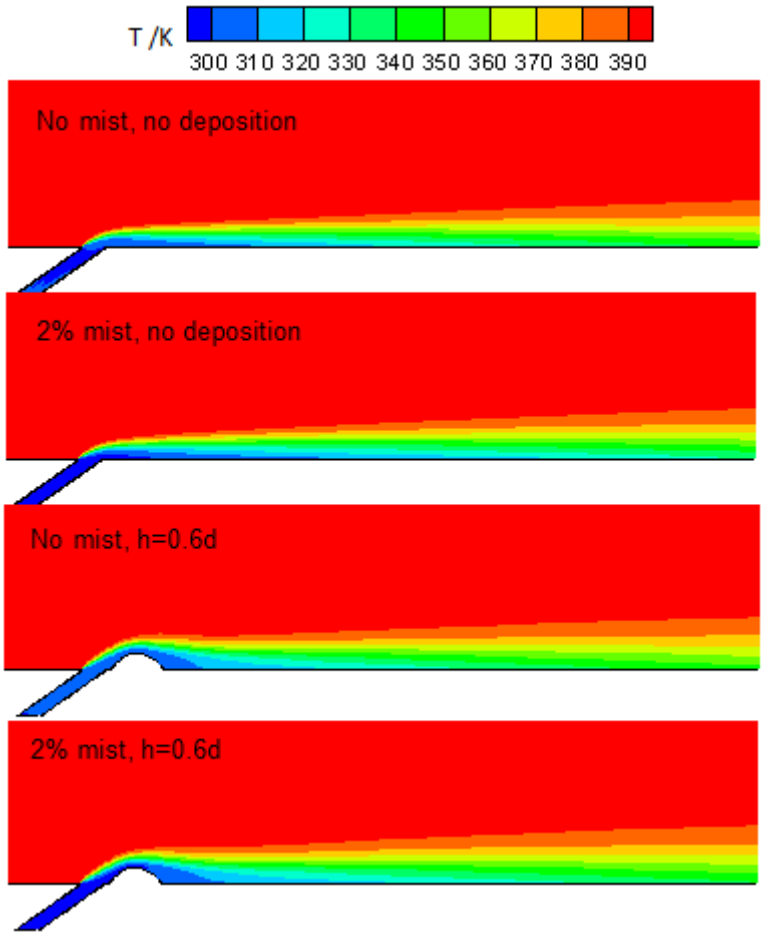

Fig. 5 Temperature distributions for 2D model with and without mist and deposition (h=0.6d)

The water droplet trajectories are predicted using a stochastic tracking method together with the consideration of the turbulent dispersion, as shown in the Figure 6. Most of the water droplets are brought toward the wall due to the turbulent dispersion, which causes improvement of the wall cooling effectiveness; some droplets fly into the mainstream, and they are evaporated due to the high temperature. The jet flow after surface deposition shows a high capacity to cool a wide wall area. To analyze the effect of surface deposition on the wall temperature, three different heights of deposition are simulated. The water droplets will occupy the region immediately after surface deposition when the deposition height is low (h=0.4d). With increase in the height of surface deposition, it can be seen that most of the droplet particles fly over downstream and there is a flow vacuum region after surface deposition. However, the vacuum region disappears when the deposition height is further increased up to 0.8d. In addition, the number of water droplets that migrate into the mainstream rises with the increase in the deposition height. As shown in Figure 6, higher deposition (h=0.8d) shows larger evaporation rate and cooling area.

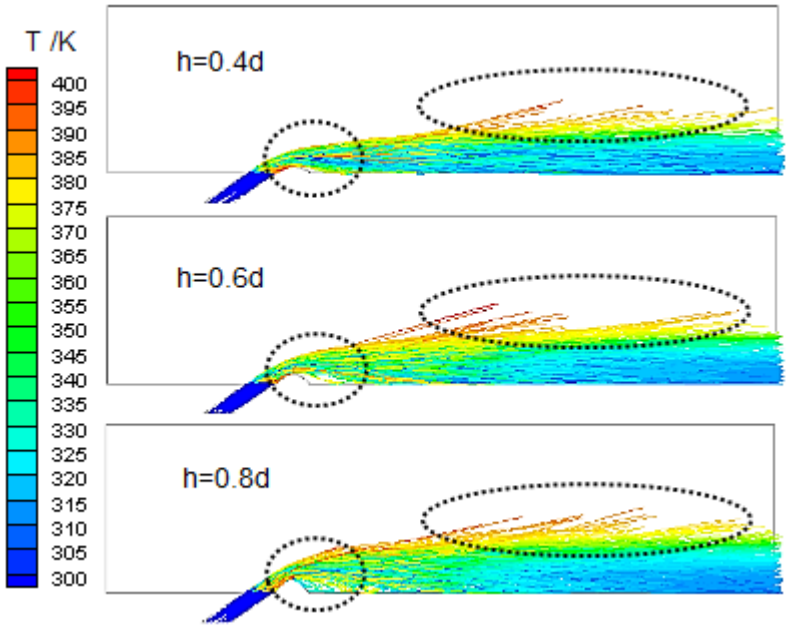

Fig. 6 Particle tracks of water droplets for 3D mist model with different deposition heights

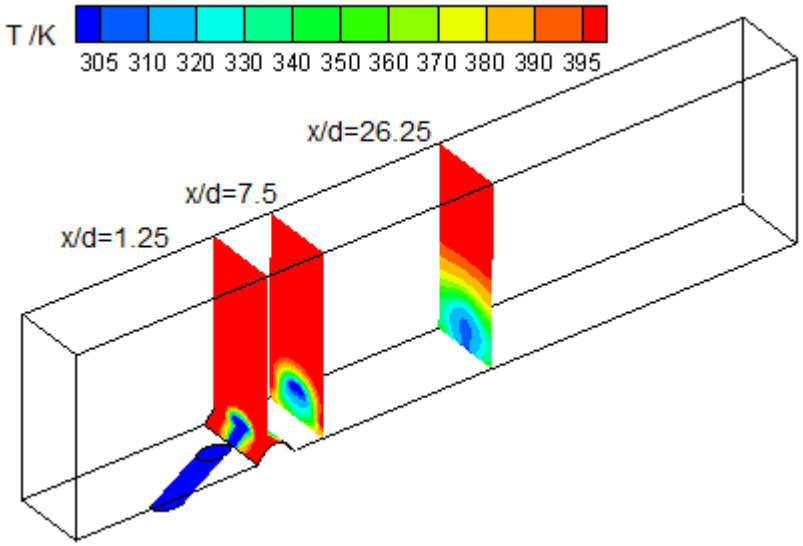

Fig. 7 Temperature distributions on three cross-sections for a mist model (h=0.8d)

Temperature distributions on three different cross-sections are shown in the Figure 7. For a mist model with surface deposition (h=0.8d), first the jet flow impinges on the surface deposition, and then it flows over the solid wall. Pressure

from the mainstream causes the jet flow to be pushed towards the wall. It can be seen that the jet flow extends to the sidewalls and the jet flow further downstream covers a larger cooling area compared to the zone near the deposition.

To obtain more details of research on mist cooling and deposition influence, temperature distributions on central cross section for both film cooling and mist cooling models, with and without surface deposition, are investigated in Figures 8 and 9. For the model without mist injection, the jet flow over a low deposition (h=0.4d) shows a strong cooling level. The coverage area is decreasing with the increase in the deposition height. The cooling capacity of the jet flow is brought down when the jet flow climbs up surface deposition. Especially in the case of higher deposition (h=0.8d), the jet flow will bend toward the wall quickly after deposition.

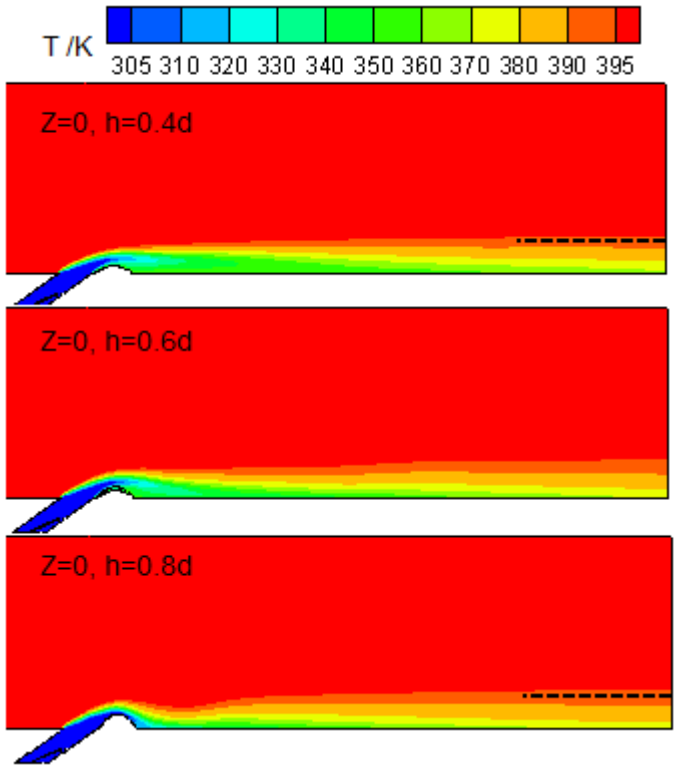

Fig. 8 Temperature distributions on mid-sections for no mist models with different depositions

From Figure 8, it can be found that the smaller deposition for model without water mist provides a lower wall temperature and a better cooling effectiveness. For the model with mist, the temperature distribution on the central cross section is shown in the Figure 9. Compared to models without mist injection, water droplets play an important role in the cooling protection for the downstream solid wall. The water mist is injected from the jet flow inlet and it enhances film cooling performance. Observing the outlet vertical direction, it is easy to see that the cooling coverage is increased by more than three times compared to no-mist cases. For the 0.4d deposition, there are several high temperature zones downstream. After deposition, the evaporation speed is increased along the flow direction. The highest deposition (h=0.8d) shows the thickest cooling coverage layer.

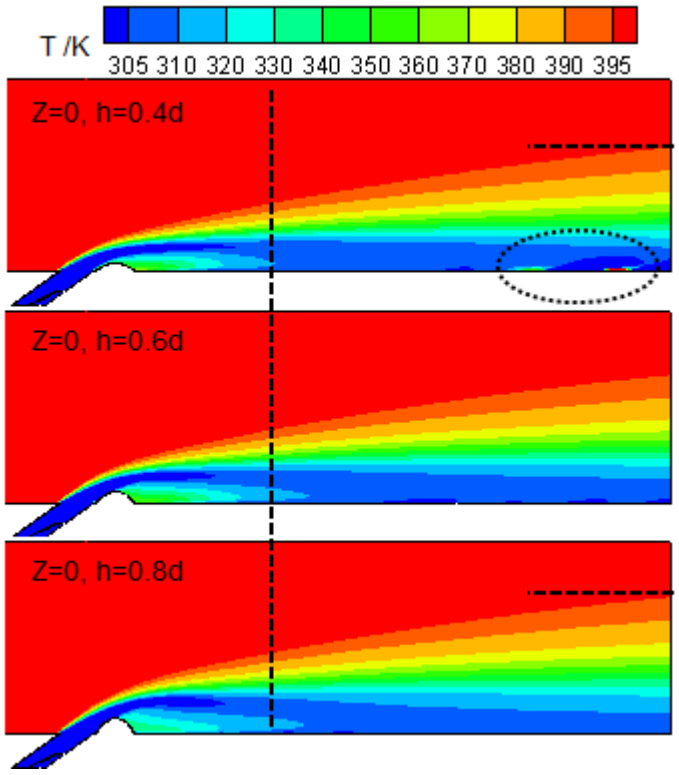

Fig. 9 Temperature distributions on mid-sections for mist models with different depositions

Figure 10 shows the average area temperature on the downstream wall centreline for cases with and without mist injection and different deposition heights. Compared to the cases without surface deposition, the average value of wall temperature for the cases with deposition is increasing. Surface deposition causes the jet flow to lift off from the zone near deposition, and the downstream cooling protection is enhanced. So the cooling range is larger than that without surface deposition. It can be found that both mist injection and surface deposition result in a temperature decrease on the downstream wall. In order to improve the cooling performance for the results of 3D models with mist injection, the average temperature on the downstream wall can be decreased by increasing the deposition height.

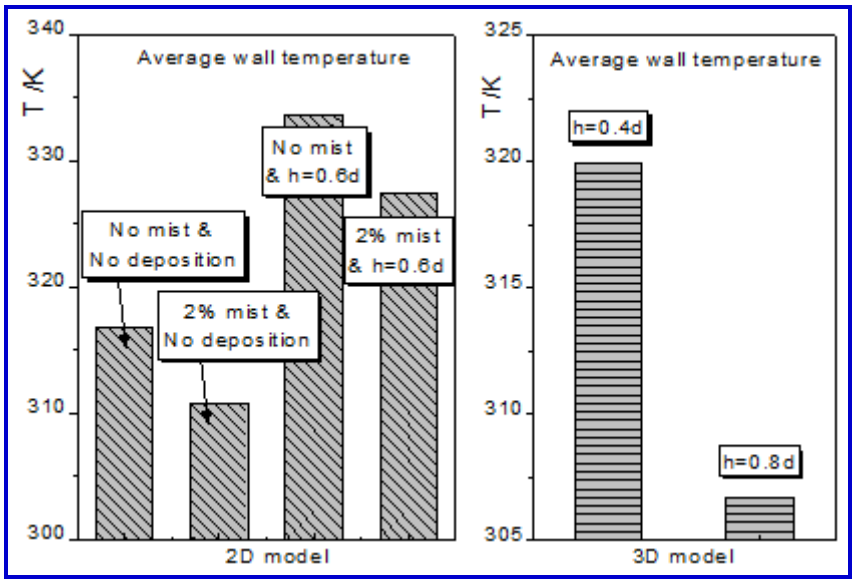

Fig. 10 Average wall temperatures on the downstream centrelines for 2D (left) and 3D (right) models

3.2 Film cooling effectiveness

To examine the performance of film/mist cooling, the adiabatic cooling effectiveness η is defined as follows:

$$\eta = \frac{\left(T_{\mathrm{i}} - T_{aw}\right)}{\left(T_{\mathrm{i}} - T_{j}\right)} \tag{12}$$

where T_{i} is the inlet temperature of the mainstream, T_{j} is the jet flow temperature, and T_{aw} is adiabatic wall temperature. The wall adiabatic cooling effectiveness for simulation models with deposition is given in Figures 11 and 12.

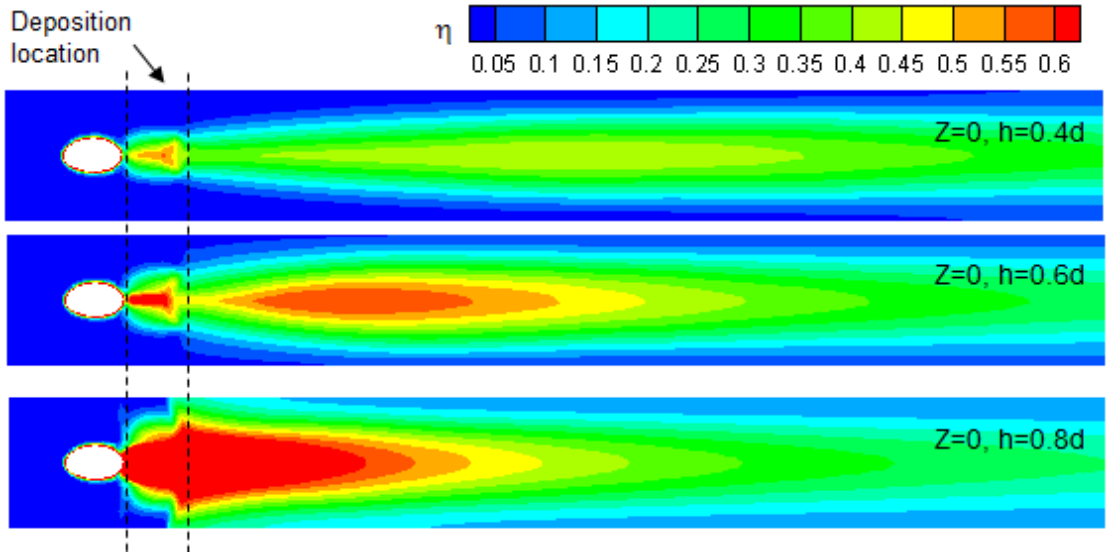

Fig. 11 Wall film cooling effectiveness for no mist models with different depositions

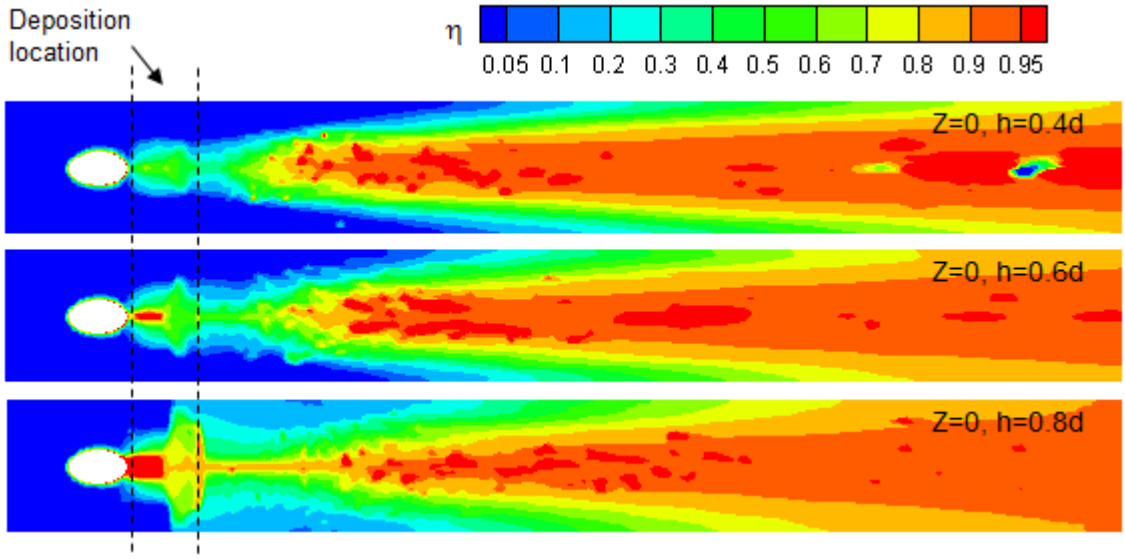

Fig. 12 Wall film cooling effectiveness for mist cooling models with different depositions

For the models without mist in the Figure 11, there is a zone with high adiabatic cooling effectiveness on the deposition surface. Moreover, the effectiveness values are rising significantly with an increase of the deposition height. High values of the adiabatic cooling effectiveness are falling down after flow passes by surface deposition. When surface deposition is high enough (h=0.8d), a high cooling protection zone emerges after deposition surface and a wide coverage area with adiabatic effectiveness values of more than 0.6 is formed. The lateral adiabatic cooling effectiveness is also enhanced by an increase in deposition height. That suggests that the cooling level on the solid wall can be improved by raising the deposition height.

Compared with the air film cooling model, adiabatic cooling effectiveness on the deposition surface is weakened in the case of mist injection. From Figure 12, the higher cooling effectiveness appears in the downstream region, and the values are even more than 0.9. Adiabatic cooling effectiveness with mist injection presents a more powerful protection than that for the single-phase (air) film cooling. The higher deposition causes lateral spread of water droplets, so the region near surface deposition shows higher values of adiabatic cooling effectiveness. When the deposition height is 0.4d, some regions of low cooling effectiveness emerge. It reveals that these locations are exposed to the mainstream, and the jet flow cooling doesn’t affect them.

4 Conclusions

Compared to air film cooling, temperature distribution near the solid wall for the mist cooling is predicted employing a discrete phase model (DPM). Film cooling characteristics with mist injection show a better cooling performance. Based on TBC surface deposition with three different heights, the local adiabatic cooling effectiveness on the wall has been investigated. Different sizes of deposition play the important effect on evaporation cooling effectiveness on the downstream wall.

For models without deposition, the adiabatic wall temperature is decreased by an inlet temperature difference of 15% after 2% mist injection into the jet flow. The results indicate that film cooling effectiveness can be improved significantly by injecting the water droplets. Moreover, the length of a low temperature zone is extended.

After deposition is taken into account, the jet flow lifts off from the wall surface, and the downstream cooling level is enhanced. Without mist injection, the coverage area is decreasing with increasing the deposition height. In other words, smaller deposition without mist injection provides a lower wall temperature and a better cooling performance. With mist injection, water droplets injected from the jet flow inlet enhance film cooling effectiveness and the higher deposition causes lateral and downstream spread of water droplets. Moreover, the cooling coverage perpendicular to the wall is increased by more than three times compared to the cases without mist injection.

5 Acknowledgments

This work is supported by the Natural Science Foundation of Hebei Province (No. E2016202266) and the Scientific Innovation Foundation for Excellent Young Scientists of Hebei University of Technology (No. 2015004).

References

[1] Benini E. Advances in Gas Turbine Technology. InTech; 2011. doi:10.5772/664.

[2] Polezhaev J. The transpiration cooling for blades of high temperatures gas turbine. Energy Convers Manag 1997;38:1123–33. doi:10.1016/S0196-8904(96)00142-2.

[3] Hao Z, Gu C. Numerical modeling for gaseous cavitation of oil film and non-equilibrium dissolution effects in thrust bearings. Tribol Int 2014;78:14–26. doi:10.1016/j.triboint.2014.04.028.

[4] Hao Z-R, Gu C-W, Ren X-D. The Application of Discontinuous Galerkin Methods in Conjugate Heat Transfer Simulations of Gas Turbines. Energies 2014;7:7857–77. doi:10.3390/en7127857.

[5] Hao Z, Gu C, Song Y. Discontinuous Galerkin Finite Element Methods for Numerical Simulations of Thermoelasticity. J Therm Stress 2015;38:983–1004. doi:10.1080/01495739.2015.1038492.

[6] Maiteh BY, Jubran BA. Effects of pressure gradient on film cooling effectiveness from two rows of simple and compound angle holes in

combination. Energy Convers Manag 2004;45:1457–69. doi:10.1016/j.enconman.2003.09.007.

[7] Koç İ , Parmaksı zogˇ lu C, Çakan M. Numerical investigation of film cooling effectiveness on the curved surface. Energy Convers Manag 2006;47:1231–46. doi:10.1016/j.enconman.2005.07.010.

[8] Asghar FH, Hyder MJ. Computational study of film cooling from single and two staggered rows of novel semi-circular cooling holes including coolant plenum. Energy Convers Manag 2011;52:329–34. doi:10.1016/j.enconman.2010.07.004.

[9] Bayraktar S, Yı lmaz T. Three-dimensional analysis of temperature field for various parameters affect the film cooling effectiveness. Energy Convers Manag 2011;52:1914–29. doi:10.1016/j.enconman.2010.10.035.

[10] Shine SR, Kumar SS, Suresh BN. Internal wall-jet film cooling with compound angle cylindrical holes. Energy Convers Manag 2013;68:54–62. doi:10.1016/j.enconman.2012.12.021.

[11] Li X, Gaddis JL, Wang T. Modeling of Heat Transfer in a Mist/Steam Impinging Jet. J Heat Transfer 2001;123:1086. doi:10.1115/1.1409262.

[12] Li X, Wang T. Simulation of Film Cooling Enhancement With Mist Injection. J Heat Transfer 2006;128:509. doi:10.1115/1.2171695.

[13] Dhanasekaran TS, Wang T. Numerical model validation and prediction of mist/steam cooling in a 180-degree bend tube. Int J Heat Mass Transf 2012;55:3818–28. doi:10.1016/j.ijheatmasstransfer.2012.02.042.

[14] Dhanasekaran TS, Wang T. Simulation of Mist Film Cooling on Rotating Gas Turbine Blades. J Heat Transfer 2012;134:011501. doi:10.1115/1.4004480.

[15] Jiang Y, Zheng Q, Dong P, Zhang H, Yu F. Research on heavy-duty gas turbine vane high efficiency cooling performance considering coolant phase transfer. Appl Therm Eng 2014;73:1177–93. doi:10.1016/j.applthermaleng.2014.09.023.

[16] Jiang Y, Zheng Q, Dong P, Yue G, Gao J. Numerical Simulation on Turbine Blade Leading-Edge High-Efficiency Film Cooling by the Application of Water Mist. Numer Heat Transf Part A Appl 2014;66:1341–64. doi:10.1080/10407782.2014.915690.

[17] Mohapatra AK, Sanjay. Thermodynamic assessment of impact of inlet air cooling techniques on gas turbine and combined cycle performance. Energy 2014;68:191–203. doi:10.1016/j.energy.2014.02.066.

[18] Bohn D, Krewinkel R. Conjugate Simulation of the Effects of Oxide Formation in Effusion Cooling Holes on Cooling Effectiveness. Vol. 3 Heat Transf. Parts A B, ASME; 2009, p. 1335–43. doi:10.1115/GT2009-59081.

[19] Sundaram N, Thole KA. Effects of Surface Deposition, Hole Blockage, and Thermal Barrier Coating Spallation on Vane Endwall Film Cooling. J Turbomach 2007;129:599. doi:10.1115/1.2720485.

[20] Ai W, Murray N, Fletcher TH, Harding S, Lewis S, Bons JP. Deposition Near Film Cooling Holes on a High Pressure Turbine Vane. J Turbomach 2012;134:041013. doi:10.1115/1.4003672.

[21] Ai W, Murray N, Fletcher TH, Harding S, Bons JP. Effect of Hole Spacing on Deposition of Fine Coal Flyash Near Film Cooling Holes. J Turbomach 2012;134:041021. doi:10.1115/1.4003717.

[22] Sundaram S, Lipkin DM, Johnson CA, Hutchinson JW. The Influence of Transient Thermal Gradients and Substrate Constraint on Delamination of Thermal Barrier Coatings. J Appl Mech 2012;80:011002. doi:10.1115/1.4007727.

[23] Kistenmacher DA, Davidson FT, Bogard DG. Realistic Trench Film Cooling With a Thermal Barrier Coating and Deposition. J Turbomach 2014;136:091002. doi:10.1115/1.4026613.

[24] Bell CM, Hamakawa H, Ligrani PM. Film Cooling From Shaped Holes. J Heat Transfer 2000;122:224. doi:10.1115/1.521484.

[25] Brittingham RA, Leylek JH. A Detailed Analysis of Film Cooling Physics: Part IV— Compound-Angle Injection With Shaped Holes. J Turbomach 2000;122:133. doi:10.1115/1.555419.

[26] Brian Edward Launder DBS. Lectures in mathematical models of turbulence. London: Academic Press; 1972.

[27] Ranz, William E. WRM. Evaporation From Drops, Part I. Chem Eng Prog 1952;48:141–6.

[28] Ranz, William E. WRM. Evaporation From Drops, Part II. Chem Eng Prog 1952;48:173–80.

[29] Li X, Wang T. Two-Phase Flow Simulation of Mist Film Cooling on Turbine Blades With Conjugate Internal Cooling. J Heat Transfer 2008;130:102901. doi:10.1115/1.2944247.

[30] Li X, Wang T. Effects of Various Modeling Schemes on Mist Film Cooling Simulation. Heat Transf. Part A, vol. 2005, ASME; 2005, p. 513–23. doi:10.1115/IMECE2005-81780.

Figures and Table captions

Fig. 1 Computational domain and hole configurations for 2D and 3D

Fig. 2 Computational meshes

Fig. 3 Grid independence study (2D with 2% mist injection)

Fig. 4 Model validation (2D with and without 2% mist injection)

Fig. 5 Temperature distributions for 2D model with and without mist and deposition (h=0.6d)

Fig. 6 Particle tracks of water droplets for 3D mist model with different deposition heights

Fig. 7 Temperature distributions on three cross-sections for a mist model (h=0.8d)

Fig. 8 Temperature distributions on mid-sections for no mist models with different depositions

Fig. 9 Temperature distributions on mid-sections for mist models with different depositions

Fig. 10 Average wall temperatures on the downstream centrelines for 2D (left) and 3D (right) models

Fig. 11 Wall film cooling effectiveness for no mist models with different depositions

Fig. 12 Wall film cooling effectiveness for mist cooling models with different depositions

Table 1 Boundary conditions